Proceedings of DETC2003
2003 ASME Design Engineering Technical Conferences
September 2-6, 2003, Chicago, IL

DETC2003/DAC-48823

PLANAR TRANSLATIONAL CABLE-DIRECT-DRIVEN ROBOTS: HARDWARE IMPLEMENTATION

Robert L. Williams II
Ohio University
Athens, OH

Jigar Vadia
Ohio University
Athens, OH

ABSTRACT

We present hardware results of a planar, translational cable-direct-driven robot (CDDR). The motivation behind this work was to present kinematics and statics modeling of the CDDR along with the method to maintain positive cable tension and implement them on CDDR hardware for experimental verification. Only translational CDDR is considered in this article; we attempt to keep zero orientation by control. We ignore gravity here because the end-effector is supported on a base plate with negligible friction. Results are presented and analyzed for two linear profiles and one circular profile.

1. INTRODUCTION

Cable-direct-driven robots (CDDRs) are a type of parallel manipulator wherein the end-effector link is supported in-parallel by *n* cables with *n* tensioning motors. In addition to the well-known advantages of parallel robots relative to serial robots, CDDRs can have lower mass and better stiffness than other parallel robots. Several CDDRs and cable-direct-driven haptic interfaces (CDDHIs) have been studied in the past. An early CDDR is the *Robocrane*[1] developed by NIST for use in shipping ports. This device is similar to an upside-down six-degrees-of-freedom (dof) Stewart platform, with six cables instead of hydraulic-cylinder legs. In this system, gravity ensures that cable tension is maintained at all times. Another CDDR is *Charlotte*, developed by McDonnell-Douglas[2] for use on International Space Station. *Charlotte* is a rectangular box driven in-parallel by eight cables, with eight tensioning motors mounted on-board (one on each corner). Four CDDHIs have been built and tested, the *Texas 9-string*[3], the *SPIDAR*[4], the 7-cable master[5], and the 8-cable haptic interface[6]. CDDRs and CDDHIs can be made lighter, stiffer, safer, and more economical than traditional serial robots and haptic interfaces since their primary structure consists of lightweight, high load-bearing cables. On the other hand, one major disadvantage is that cables can only exert tension and cannot push on the end-effector.

All of the devices discussed above are designed with actuation redundancy, i.e. more cables than wrench-exerting degrees-of-freedom (except for the *Robocrane*[1], where cable tensioning is provided by gravity) in attempt to avoid configurations where certain wrenches require an impossible compression force in one or more cables. Despite actuation redundancy, there exist subspaces in the potential workspace where some cables can lose tension. This problem can be exacerbated by CDDR dynamics[7]. Roberts et al.[8] developed an algorithm for CDDRs to predict if all cables are under tension in a given configuration while supporting the robot weight only. They also present the inverse kinematics and fault tolerance of Charlotte-type[2] CDDRs, but no dynamics modeling is presented. R. L. Williams II et al.[9] developed CDDHI design with regard to wrenches with only positive cable tensions and with regard to avoiding cable interference. They found that cable interference dominates.

Choe et al.[10] present stiffness analysis for wire-driven robots. Wire driven robots must provide stiffness in all 6 Cartesian degrees of freedom even if motion is in a subspace of the general case. For the CDDR considered in the current article the planar end effector is supported on a plane; thus only the *x*, *y*, and rotation about *z* freedoms must provide stiffness from the cable drive systems. Kock and Schumacher[11] have implemented a parallel robot (not cable-suspended) with actuation redundancy. They use this actuation redundancy to avoid backdriving the gear boxes and also to allow torque optimization. Barette and Gosselin[12] present general velocity and force analysis for planar cable-actuated mechanisms. They introduce and determine dynamic workspace, dependent on end-effector accelerations.

Most proposed CDDRs and CDDHIs involve both translational and rotational motion of the end-effector link guided by cables. (An exception is the *SPIDAR*[4], which is a spatial 4-cable haptic interface reading translations only and providing three Cartesian forces (no moments) to the human finger.) All CDDRs and CDDHIs with translational and rotational motion suffer from the potential of cable interference and reduced statics workspaces wherein some negative cable tensions would be required, which is infeasible. R. L. Williams II et al[7] proposed a model to provide translational motion and forces by cables and the rotational motion and moments by a serial wrist mechanism mounted at the end-effector of the translational CDDR. They proposed a cross cable configuration to ensure that the translational CDDR end-effector has sufficient stiffness in all directions to resist the rotational moments.

This article describes a planar four-cable CDDR, followed by kinematics modeling, statics modeling, a method for attempting to maintain positive cable tensions, and a discussion of the statics workspace. The article then presents hardware implementation of these theories using linear and circular trajectory generation examples.

2. CABLE-DIRECT-DRIVEN ROBOTS (CDDRs)

In this article a CDDR consists of a single end-effector rigid body supported in parallel by *n* cables controlled by *n* tensioning actuators. Figure 1 shows the planar 4-cable CDDR kinematics diagram. We are implementing the concept of hybrid CDDRs[7], where the translational freedoms are provided by the *n*=4 cables and the rotational freedoms can be provided by a serial wrist mechanism mounted to the translational CDDR end-effector. We are considering

only the translational portion of the problem here; we will attempt to keep zero orientation by control (ϕ= 0 for all motion; ϕ, not shown in Figure. 1, is the angle between the horizontal end-effector side *a* and the horizontal ground link L_B). If the end-effector is supported by a base plate in the *XY* plane, the cross-cable configuration of Figure. 1 is sufficient in general to resist moments about the *Z* axis from a serial wrist mechanism consisting of a single revolute joint rotating about the *Z* axis, mounted to the end-effector centroid.

For 3-dof planar motions (2 translations *XY* and 1 rotation about *Z*) there must be at least three cables. Since cables can only exert tension on the end-effector, there must be more cables to avoid configurations where the robot cables can be slack and lose control. Figure 1 represents one degree of actuation redundancy, i.e. four cables to achieve the three Cartesian degrees-of-freedom $\mathbf{X} = \{x \quad y \quad \phi = 0\}^T$. This scenario represents actuation redundancy but not kinematic redundancy. That is, there is an extra motor which provides infinite choices for applying 3-dof Cartesian wrench vectors, but the moving rigid body has only three Cartesian degrees-of-freedom $\mathbf{X} = \{x \quad y \quad \phi\}^T$.

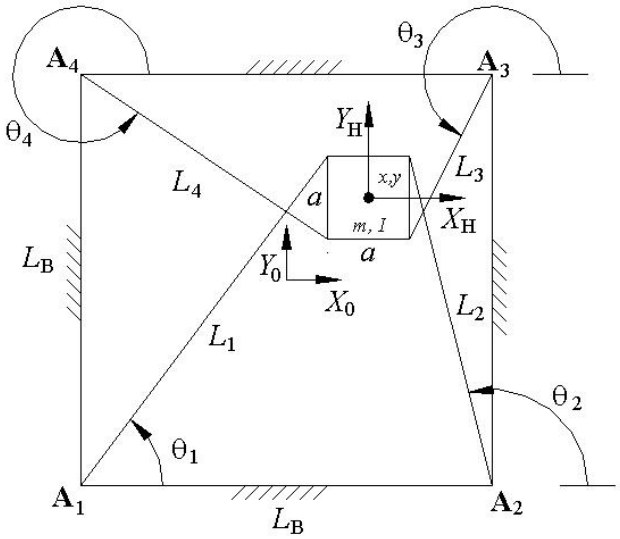

Figure 1. Planar 4-Cable CDDR Diagram

Figure 1 shows the inertially-fixed reference frame {0} whose origin is the centroid of the base square. The base square has sides of fixed length L_B. Each cable is passed through the ground link at the fixed points $\mathbf{A}_i = \{A_{ix} \quad A_{iy}\}^T$. The length of each cable is denoted as L_i, and the cable angles are θ_i ($i = 1, \cdots, 4$). The moving end-effector frame {H} is also shown in Figure. 1. Note vector $\{x \quad y\}^T$ gives the position of {H} with respect to the {0} origin, expressed in {0} coordinates. The cable pulley radius for each actuator is r_i ($i = 1, \cdots, 4$; not shown in Figure. 1).

Theoretically the end-effector center can reach any *xy* point within the base square (reduced on all sides by half the end-effector dimension, *a*/2), if cable lengths can go to zero. A singular condition exists when the edge of the square end-effector aligns with an edge of the base square. In this case two adjacent cables align with the base plate edge; infinite force is required in the two adjacent cables to move the end-effector normal to the aligned cables. The other two cables cannot push so motion is restricted to this reduced base square; large cable tensions will be required as this edge of motion is approached.

Cable interference is a potential problem in CDDRs. Using crossed cables as shown in Figure. 1, there will always be cable/cable contact for all motion; to avoid this problem either select low-friction cable materials to allow cables to slide freely over each other, or mount the cables in different planes, if the base plate sufficiently supports the end-effector. In the design of Figure 1, cable/end-effector interference is non-existent in the useful motion range if we succeed in maintaining orientation ϕ= 0 by control. In the singularities at the edge of the useful motion range, two cables will have just touched the square end-effector side, even with ϕ= 0. The potential exists for interference between cables and workspace items and/or humans, but this problem can be minimized by design in the case of planar CDDRs

3. CDDR KINEMATICS MODELING

Kinematics modeling is concerned with relating the active joint variables and rates to the Cartesian pose and rate variables of the end-effector. The intermediate, passive cable angles and rates are also involved. Assuming all cables always remain in tension, CDDR kinematics is similar to in-parallel-actuated robot kinematics (e.g.[14,15]); however, with CDDRs the joint space is overconstrained with respect to the Cartesian space.

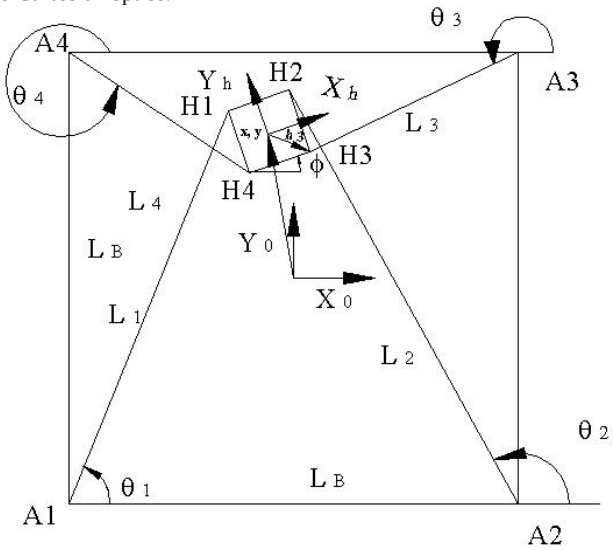

Figure 2. Planar 4-Cable CDDR Kinematics Diagram

The inverse position kinematics problem is stated: given the Cartesian position $\mathbf{X} = \{x \quad y \quad \phi\}^T$ calculate the cable lengths L_i. The solution is simply calculating the Euclidean norm between the moving point $\mathbf{X} = \{x \quad y \quad \phi\}^T$ and each fixed ground link vertex $\mathbf{A}_i$. $\mathbf{h}_i$ is the position vector from the origin of {**H**} to the i^{th} cable connection, expressed in {**H**} coordinates (only $\mathbf{h}_3$ is shown in Figure. 2)

$$L_i = \sqrt{(x - A_{ix} + h_{ix}c\phi - h_{iy}s\phi)^2 + (y - A_{iy} + h_{ix}s\phi + h_{iy}c\phi)^2} \qquad i = 1, \cdots, n \qquad (1)$$

For use in velocity kinematics and statics, we require the cable angles:

$$\theta_i = tan^{-1}\left(\frac{y - A_{iy} + h_{ix}s\phi + h_{iy}c\phi}{x - A_{ix} + h_{ix}c\phi - h_{iy}s\phi}\right) \qquad i = 1, \cdots, n \qquad (2)$$

The quadrant-specific inverse tangent function must be used in Eq. 2.

The forward pose kinematics problem requires the solution of overconstrained coupled nonlinear equations and is more difficult.

A Newton-Raphson numerical solution has been employed, where the overconstrained Moore-Penrose pseudoinverse is used in the iteration. The CDDR inverse velocity Jacobian matrix is closely related to the Newton-Raphson Jacobian matrix and the statics Jacobian matrix. These kinematics solutions are presented in[6] and will not be repeated here.

4. CDDR STATICS MODELING

In this article, the workspace wherein all cables are under positive tension while exerting all possible Cartesian wrenches is called the statics workspace. Statics modeling and attempting to maintain positive cable tension for all wrenches are presented in this section. We use a simple method to determine the extent of the statics workspace, i.e. the workspace wherein all possible end-effector wrenches can be resisted with only positive cable tensions.

4.1 Statics Modeling

This section presents statics modeling for planar CDDRs. For static equilibrium the sum of external forces and moments exerted on the end-effector by the cables must equal the resultant external wrench exerted on the environment (or, the wrench exerted by a serial wrist mechanism acting on the environment must react on the CDDR end-effector). Figure 3 shows the statics free-body diagram for the planar 4-cable CDDR.

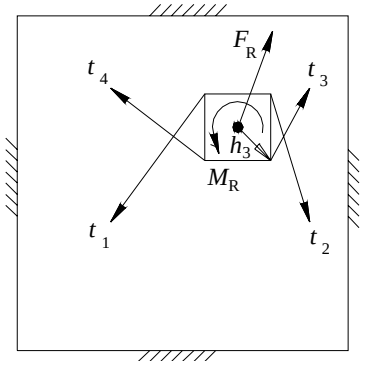

Figure 3. Planar 4-Cable CDDR Statics Diagram

The statics equations are:

$$\sum_{i=1}^{4}\mathbf{t}_i = -\sum_{i=1}^{4} t_i\hat{\mathbf{L}}_i = \mathbf{F}_R \qquad \sum_{i=1}^{4}\mathbf{m}_i = \sum_{i=1}^{4}\left({}^0_H\mathbf{R}\mathbf{h}_i\right)\times\mathbf{t}_i = \mathbf{M}_R \tag{3}$$

In this article gravity is ignored because it is assumed to be perpendicular to the CDDR plane; we assume the end-effector is supported on a base plate with negligible friction. The definition of frames {**0**} and {**H**} are given in Figure. 3. In (3), t_i is the cable tension applied to the i^{th} cable (in the negative cable length unit direction $\hat{\mathbf{L}}_i$ because $\mathbf{t}_i$ must be in tension); ${}^0_H\mathbf{R}$ is the orthonormal rotation matrix relating the orientation of {**H**} to {**0**} (nominally, ${}^0_H\mathbf{R} = \mathbf{I}_3$ since we are controlling for zero orientation, ϕ=0); $\mathbf{h}_i$ is the position vector from the origin of {**H**} to the i^{th} cable connection, expressed in {**H**} coordinates (only $\mathbf{h}_3$ is shown in Figure. 3); and $\mathbf{F}_R$ and $\mathbf{M}_R$ are the resultant vector force and moment (taken together, wrench) exerted on the environment. Substituting the above terms into (3) yields:

$$\mathbf{S}\mathbf{T} = \mathbf{W}_R \tag{4}$$

$\mathbf{T} = \{t_1 \quad t_2 \quad t_3 \quad t_4\}^T$ is the vector of scalar cable forces, $\mathbf{W}_R = \{\mathbf{F}_R \quad \mathbf{M}_R\}^T = \{F_{Rx} \quad F_{Ry} \quad M_{Rz}\}^T$ is the resultant external end-effector wrench vector (expressed in {**0**} coordinates but felt at the origin of {**H**}), and the 3*x*4 Statics Jacobian matrix $\mathbf{S}$ (expressed in {**0**} coordinates) is:

$$\mathbf{S} = \begin{bmatrix} -\hat{\mathbf{L}}_1 & -\hat{\mathbf{L}}_2 & -\hat{\mathbf{L}}_3 & -\hat{\mathbf{L}}_4 \\ \hat{\mathbf{L}}_1\times{}^0_H\mathbf{R}\mathbf{h}_1 & \hat{\mathbf{L}}_2\times{}^0_H\mathbf{R}\mathbf{h}_2 & \hat{\mathbf{L}}_3\times{}^0_H\mathbf{R}\mathbf{h}_3 & \hat{\mathbf{L}}_4\times{}^0_H\mathbf{R}\mathbf{h}_4 \end{bmatrix} \tag{5}$$

The specific (5) expressions for the Figure. 1 CDDR are:

$$\mathbf{S} = \begin{bmatrix} -c\theta_1 & -c\theta_2 & -c\theta_3 & -c\theta_4 \\ -s\theta_1 & -s\theta_2 & -s\theta_3 & -s\theta_4 \\ c\theta_1 h_{1y} - s\theta_1 h_{1x} & c\theta_2 h_{2y} - s\theta_2 h_{2x} & c\theta_3 h_{3y} - s\theta_3 h_{3x} & c\theta_4 h_{4y} - s\theta_4 h_{4x} \end{bmatrix} \tag{6}$$

where $\mathbf{h}_i = \{h_{ix} \quad h_{iy}\}^T$, $c\theta_i = cos\,\theta_i$, and $s\theta_i = sin\,\theta_i$. Equation (6) assumes that the orientation is $\phi = 0$ for all pseudostatic motion; otherwise each third row term of (6) is: $c\theta_i\left(h_{ix}s\phi + h_{iy}c\phi\right) - s\theta_i\left(h_{ix}c\phi - h_{iy}s\phi\right)$. The statics equations (4) can be inverted in an attempt to resist general (in this article, planar) Cartesian wrenches while maintaining positive cable tension. This work is presented in the next subsection.

4.2 Maintaining Positive Cable Tension

For CDDRs with actuation redundancy, (4) is underconstrained which means that there are infinite solutions to the cable tension vector $\mathbf{T}$ to exert the required Cartesian wrench $\mathbf{W}_R$. To invert (4) (solving the required cable tensions $\mathbf{T}$ given wrench $\mathbf{W}_R$) we adapt the well-known particular and homogeneous solution from rate control of kinematically-redundant serial manipulators:

$$\mathbf{T} = \mathbf{S}^+\mathbf{W}_R + \left(\mathbf{I}_n - \mathbf{S}^+\mathbf{S}\right)\mathbf{z} \tag{7}$$

where $\mathbf{I}_n$ is the *nxn* identity matrix, **z** is an arbitrary *n*-vector, and $\mathbf{S}^+ = \mathbf{S}^T\left(\mathbf{S}\mathbf{S}^T\right)^{-1}$ is the *n*x3 underconstrained Moore-Penrose pseudoinverse of **S**. The first term of (7) is the particular solution to achieve the desired wrench, and the second term is the homogeneous solution that projects **z** into the null space of **S**.

For CDDRs with one degree of actuation redundancy (the case in this article), the positive cable tension method of Shen et al.[13] is adapted to determine the extent of the statics workspace. For actuation redundancy of degree one, an equivalent expression for (7) is:

$$\mathbf{T} = \begin{Bmatrix} t_{P1} \\ t_{P2} \\ t_{P3} \\ t_{P4} \end{Bmatrix} + \alpha\begin{Bmatrix} n_1 \\ n_2 \\ n_3 \\ n_4 \end{Bmatrix} \tag{8}$$

where the particular solution $\mathbf{S}^{+}\mathbf{W}_R$ is the first term in (8) and the homogeneous solution is expressed as the kernel vector **N** of **S** ($\mathbf{N} = \{n_1 \quad n_2 \quad n_3 \quad n_4\}^T$) multiplied by arbitrary scalar α.

The method we adapt from Shen et al.[13] to determine if a given point lies within the statics workspace for a given CDDR is simple. To ensure positive tensions t_i on all cables $i = 1, \cdots, 4$, *for all possible exerted forces and moments*, it is necessary and sufficient that all kernel vector components (n_i, $i = 1, \cdots, 4$) have the same sign. That is, for a given point to lie within the statics workspace, all $n_i > 0$ OR all $n_i < 0$ ($i = 1, \cdots, 4$). If one of these two conditions is satisfied, regardless of the particular solution, we can find a scalar α in (8) which guarantees that all cable tensions **T** are positive by adding (or subtracting) enough homogeneous solution. Note a strict inequality is required; if one or more $n_i = 0$, the CDDR configuration in question does not lie within the statics workspace. This method is simple but powerful since we needn't consider specific wrenches: it works for *all possible wrenches*. It should also be noted that while we demonstrate this method for the planar 4-cable CDDR, it is applicable to any planar and spatial CDDR with one degree of actuation redundancy.

A symbolic expression for the kernel vector (null space basis) of the 4-cable CDDR (with $\phi = 0$) is:

$$\mathbf{N} = \begin{Bmatrix} n_1 \\ n_2 \\ n_3 \\ n_4 \end{Bmatrix} \tag{9}$$

where

$$\begin{Bmatrix} n_1 \\ n_2 \\ n_3 \\ n_4 \end{Bmatrix} = \begin{Bmatrix} cos(\theta_2 - \theta_3 + \theta_4) - cos(\theta_2 - \theta_3 - \theta_4) + sin(\theta_2 - \theta_3 + \theta_4) - sin(\theta_2 + \theta_3 - \theta_4) \\ cos(\theta_1 - \theta_3 - \theta_4) - cos(\theta_1 + \theta_3 - \theta_4) + sin(\theta_1 + \theta_3 - \theta_4) - sin(\theta_1 - \theta_3 + \theta_4) \\ cos(\theta_1 + \theta_2 - \theta_4) - cos(\theta_1 - \theta_2 - \theta_4) + sin(\theta_1 - \theta_2 - \theta_4) + sin(\theta_1 - \theta_2 + \theta_4) \\ cos(\theta_1 - \theta_2 + \theta_3) - cos(\theta_1 + \theta_2 - \theta_3) - sin(\theta_1 - \theta_2 + \theta_3) - sin(\theta_1 - \theta_2 - \theta_3) \end{Bmatrix}$$

Now, the allowable cable angle ranges are $0 < \theta_1 < 90^\circ$, $90^\circ < \theta_2 < 180^\circ$, $180^\circ < \theta_3 < 270^\circ$, and $270^\circ < \theta_4 < 360^\circ$. The analysis based on these allowable angles ranges, by careful consideration of sums/differences of the three distinct angle combinations in each row of (21) is shown in Table 1. By substitution of these results in (21), it can be proved easily that the sign of ALL n_i components is always the same (negative in this case), $i = 1, \cdots, 4$.

Therefore, *the entire allowable kinematic workspace of the base square is also the statics workspace*! Now, when the edge of the end-effector square is aligned with an edge of the base square, two components $n_i = 0$ and thus the allowable statics workspace is the base square, reduced by *a*/2 (half the end-effector side) on all sides. This edge singularity condition was discussed earlier in Section 2. At all points outside of the base square, all components of the kernel vector **N** do not have the same sign so outside the useful region of the base square is also outside of the statics workspace. This statics workspace discussion holds only for $\phi = 0$, the nominal case of the planar translational CDDR. In previous work by[9], it was discovered that the statics workspace is extremely limited when considering general ϕ rotations.

For real-time pseudostatic control of a planar CDDR with one degree of actuation redundancy, the cable tensions for control are calculated by (8) and (9), choosing α so that one component of **T** is zero (or, a small positive tension value) and the remaining terms are positive.

n1	**Cos**	**Sin**
$180 < \theta_2 - \theta_3 + \theta_4 < 270$	-Ve	-Ve
$0 < \theta_2 + \theta_3 - \theta_4 < 90$	+Ve	+Ve
$-360 < \theta_2 - \theta_3 - \theta_4 < -450$	+Ve	-Ve
n2	**Cos**	**Siṇ**
$90 < \theta_1 - \theta_3 + \theta_4 < 180$	-Ve	+Ve
$-450 < \theta_1 - \theta_3 - \theta_4 < -540$	-Ve	-Ve
$-90 < \theta_1 + \theta_3 - \theta_4 < 0$	+Ve	-Ve
n3	**Cos**	**Siṇ**
$-360 < \theta_1 - \theta_2 - \theta_4 < -450$	+Ve	-Ve
$180 < \theta_1 - \theta_2 + \theta_4 < 270$	-Ve	-Ve
$-180 < \theta_1 + \theta_2 - \theta_4 < -90$	-Ve	-Ve
n4	**Cos**	**Siṇ**
$90 < \theta_1 - \theta_2 + \theta_3 < 180$	-Ve	+Ve
$-270 < \theta_1 - \theta_2 - \theta_3 < -360$	+Ve	+Ve
$-90 < \theta_1 + \theta_2 - \theta_3 < 0$	+Ve	-Ve

Table 1 : Kernel Vectors Analysis

5. Hardware Implementation

This section presents hardware implementation of the kinematics and statics modeling along with the method to maintain positive cable tensions, which we discussed in section 3 and 4. Figure 4 shows the CDDR hardware used for experimentation. Hardware consists of an end-effector with ball transfers below to reduce friction, four pulleys, four DC servomotors with angle feedback mechanism, an aluminum base plate, a power supply and four amplifiers. The base square has side L_B = 0.70 *m* and the end-effector square has side *a* = 0.10 *m*. Hardware was interfaced with the computer using Quanser MultiQ PCI data acquisition boards. Matlab, Simulink and Wincon 3.2 were used for real time control of the robot. Low friction nylon cables were used to allow cables to slide freely over each other. Four guides were placed on all four corners to keep all four cables at same height.

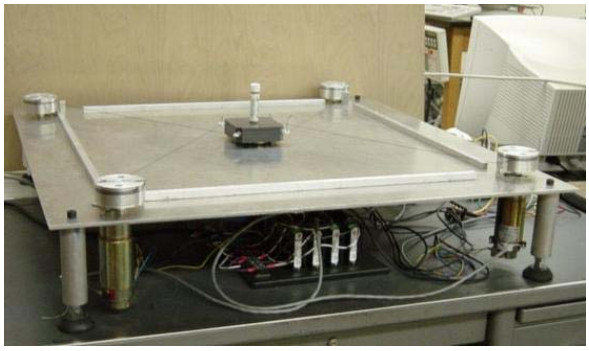

Figure 4. CDDR Hardware

5.1 Control Architecture

The control architecture of the CDDR system is shown in Figure 5. X is commanded pose (x, y, ϕ), L is the commanded leg lengths, Θ is the vector of cable angles, N is kernel vector as given by equation 9 and α is a scalar quantity. In the control architecture, the inverse kinematics transforms the commanded pose into commanded leg lengths and cable angles using equation 1 and equation 2 respectively. Kernel vectors can be found using equation-9. The scalar α can be found by dividing the minimum allowable cable tension (0.3 N from our experiment) by the minimum kernel vector. Commanded cable lengths L and kernel vectors N are provided to the four independent length PD controllers. Cable lengths are calculated online using the encoder feedback for each cable pulley. These lengths are also used offline as the inputs to the forward position kinematics solution to calculate Cartesian position **X**.

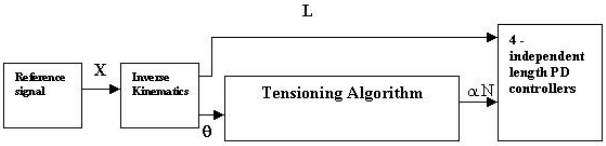

Figure 5. Control Architecture

5.2 Results

The experiments aimed at generating two linear profiles: move the end-effector from the origin (center of the plate) to (0.10,0) and (0.10,0.10) and one circular profile: trace a circle of 0.15 meter radius starting from (0.15,0) keeping center of the base plate as origin.

5.2.1 Linear Trajectory Generation. The end-effector was commanded to move from: The origin (center of the base plate) to (0.10, 0) and (0.10,0.10) in one second while attempting to maintain $\phi = 0$ for all motion. As commanded motion was symmetrical to the x-axis for the first case, desired cable lengths L1 and L4 as well as L2 and L3 were the same. Therefore in the Figure 6 desired lengths for cables L3 and L4 covers those of cables L2 and L1. Cables L2 and L3 were required to pull the cables while cables L1 and L4 were required to release the cables but keep minimum tension to avoid slack and hence maintain control of the robot. Figure 6 shows the commanded and actual length control of the robot. Cables L1 and L4 were required to release the cables and therefore increase in lengths of the cable L1 and L4, which can be observed in the Figure 6. Cables L2 and L3 were required to pull the cables and therefore decrease in lengths of the cables L2 and L3, which can also be observed in the Figure 6.

For the second case, commanded motion was symmetrical to the xy-axis therefore all desired lengths were different unlike the first case. L1 and L2 were required to release the cables but keep minimum tension to avoid slack and hence maintain control of the robot. Cables L3 and L4 were required to pull the cables. L1 and L2 were required to release the cables therefore increase in their lengths can be observed in Figure 7. Cables L3 and L4 were required to pull the cables therefore decrease in their lengths can be observed. Desired cable length L4 is covered by the actual value in Figure 7 for most of the part. Figure 8 shows the commanded and actual Cartesian control of the robot for the linear trajectory (0,0) to (0.10,0). As desired motion in y-direction as well as commanded rotational angle phi is zero phi-desired in Figure 8 covers the y-desired. Figure 9 shows the commanded and actual Cartesian control of the robot for the linear trajectory (0,0) to (0.10,0.10). As desired motion is symmetrical to x-y axis, desired x and y motion are overlapping. There is a significant error in phi initially, which reduces gradually.

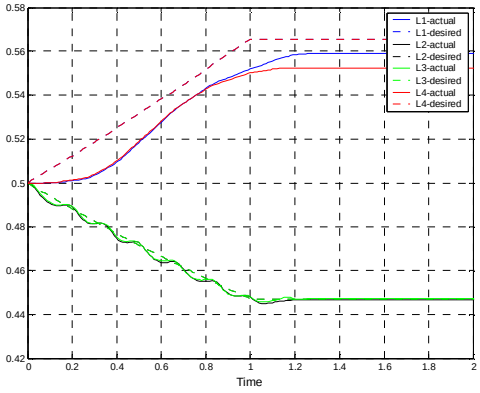

Figure 6: Length Control for the Linear Trajectory (0,0) to (0.10,0)

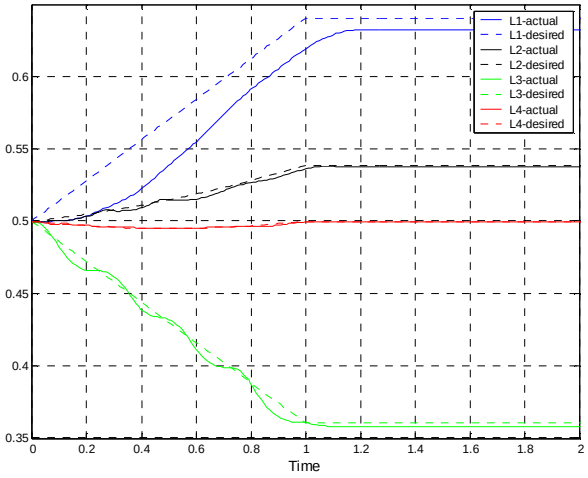

Figure 7: Length Control for Linear Trajectory (0,0,) to (0.10,0.10)

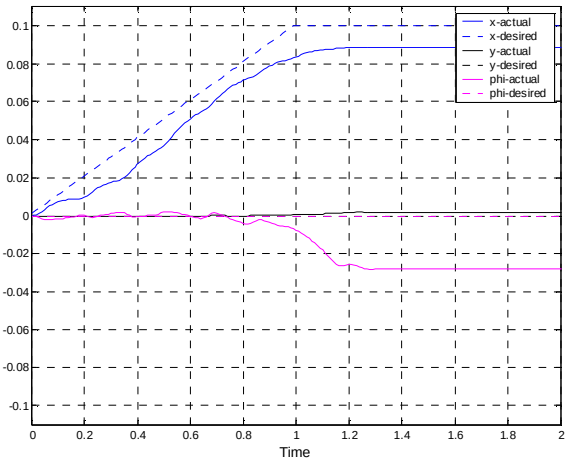

Figure 8: Cartesian Control for Linear Trajectory (0,0) to (0.10,0)

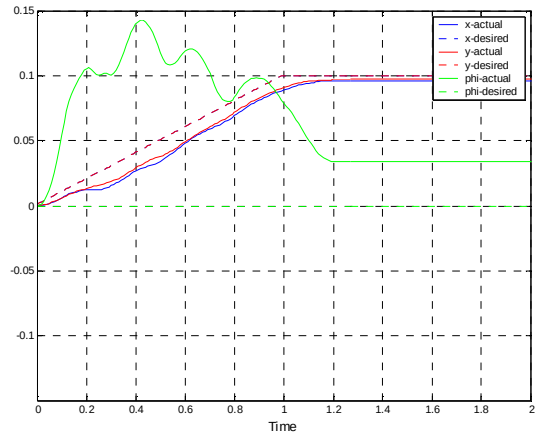

Figure 9:Cartesian Control for Linear Trajectory (0,0) to (0.10,0.10)

The errors in the Cartesian control of the robot for both cases are shown in the Figure 10 and Figure 11. The errors in x and y are in meters while the Phi error is in radians. Figure 12 and Figure 13 shows the trajectory achieved by the CDDR hardware in real time compared to the desired trajectory.

As it can be seen in the Figure, the end-effector could not reach to the exact commanded x coordinate which explains the positive error ($X_{commanded}$-X_{actual}) in Figure 10. As the end-effector moved towards the workspace boundary it approached to singularity. The cables needed infinite force to pull the end-effector towards the boundary of the workspace. The end-effector moves in y direction while commanded trajectory in y-direction is zero for this trajectory, which explains the negative error ($Y_{commanded}$ -Y_{actual}) for y coordinate in Figure 10. Figure 10 also shows the positive error for the rotational angle phi, which means that the end-effector rotated clockwise about the z-axis while attempting the linear trajectory. The error in phi can be reduced if the Cartesian controller could be implemented instead of independent length controller. Cartesian controller needs online Cartesian feedback from the CDDR, which can be achieved by introducing vision system in future.

For the second case, the end-effector is commanded to move from the origin to (0.10,0.10) .The end-effector movement in x-y direction is very close to the commanded motion, it can be seen in the Figure 13. During this motion the end-effector was approaching the corner of the workspace but it was not approaching to singularity because cable in that corner could pull the end-effector in the same direction.

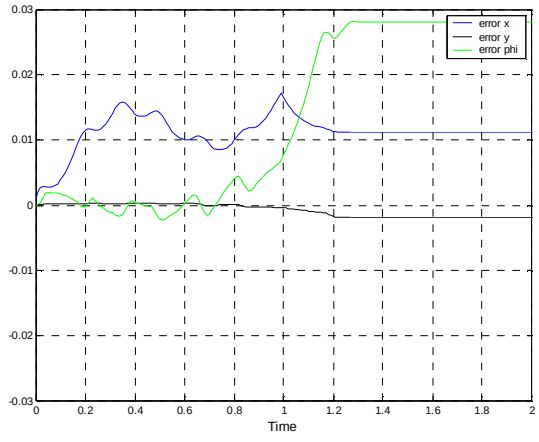

Figure 10: Cartesian Control Errors for Linear Trajectory (0,0) to (0.10,0)

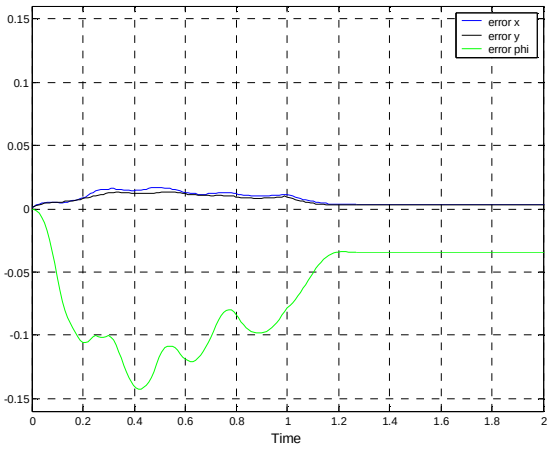

Figure 11:Cartesian Control Errors for Linear Trajectory (0,0) to (0.10,0.10)

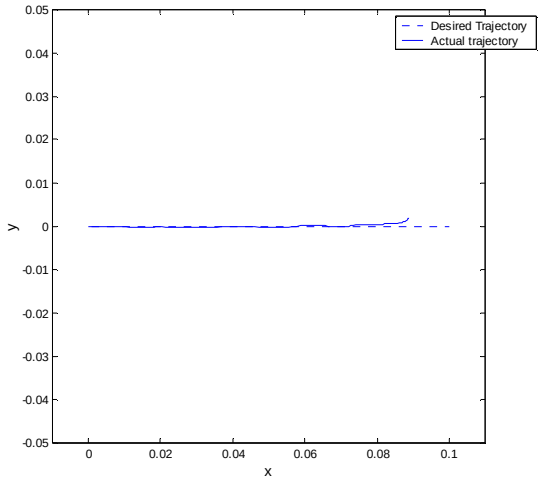

Figure 12:Linear Trajectory Generation: (0,0) to (0.1,0)

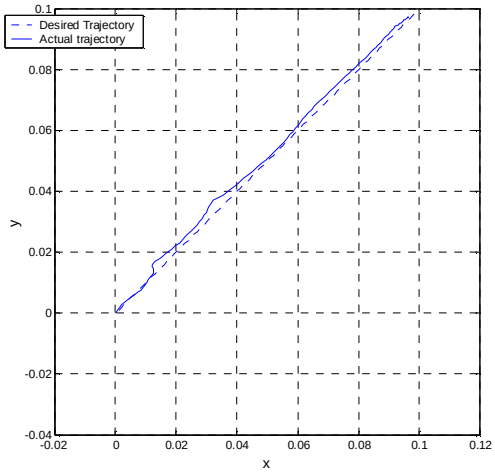

Figure 13:Linear Trajectory Generation: (0,0) to (0.10,0.10)

5.2.2 Circular Trajectory Generation. In this experiment the end-effector was commanded to trace a circle of r = 0.15 meter radius and centered at the origin (center of the base plate) while attempting to

maintain $\phi = 0$ for all motion in 10 seconds. Angle γ was defined as the polar angle for the circle; it was measured using the right-hand from the right horizontal to the circle radius. For 'smooth' motion starting and ending at rest, trajectory generation techniques were adopted[17]: We required that angle γ starts at zero and ends at 360° during the 10 *sec* motion; also, we required that $\dot{\gamma} = \ddot{\gamma} = 0$ at the start and end of motion, for 'smoothness'. These conditions yielded a 5^{th} order polynomial for angle γ: $\gamma(t) = (27/1250)t^5 - (27/50)t^4 + (18/5)t^3$ (*deg*). The associated commanded (reference) Cartesian pose for use in the controller architecture were x = r.cos(γ) and y = r.sin(γ). The commanded Cartesian angular value was $\phi = 0$ for all motion. Figure 14 shows the commanded and actual length control for the circular trajectory. Figure 15 shows the commanded and actual Cartesian control of the circular trajectory. Figure 16 shows the Cartesian control errors and Figure 17 shows the simulation of the actual trajectory generated by the end-effector compared to the desired circle Commanded trajectory is very close to the singularity region, so it can be observed easily that during most of the motion the actual trajectory is inside the desired trajectory, as cables needed very high force to move the end-effector close to the workspace boundary. Implementing dynamics controller can reduce errors. Introducing Cartesian controller can also reduce the errors in phi as already discussed in 5.2.1.

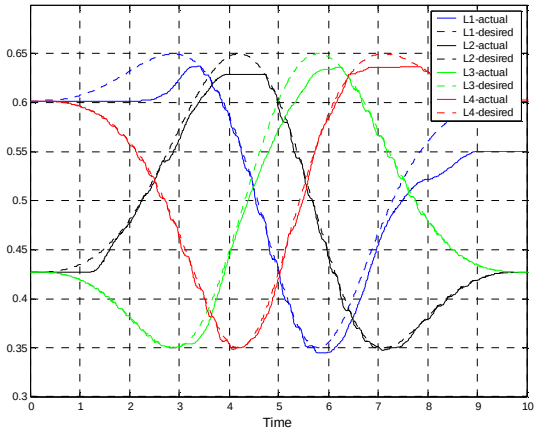

Figure 14: Length Control for Circular Trajectory

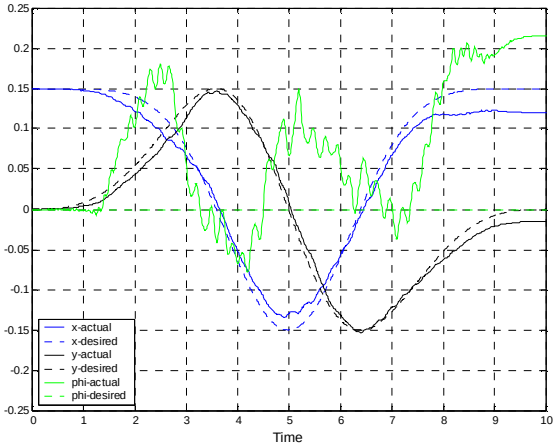

Figure 15: Cartesian Control for Circular Trajectory

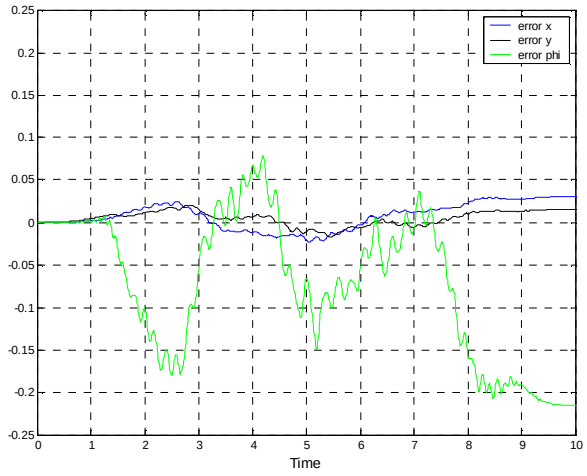

Figure 16: Cartesian Control Errors for Circular Trajectory

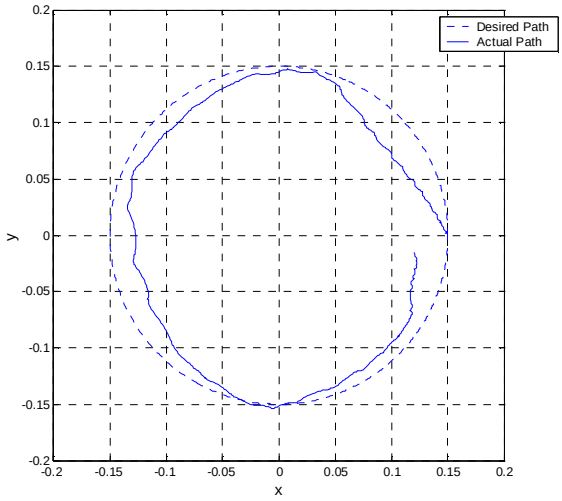

Figure 17: Circular Trajectory Generation

5.2.3 Repeatability

Repeatability is the ability of the robot to repeatedly position itself when asked to perform a task multiple times. Repeatability of the CDDR was measured by generating a circular trajectory repeatedly (seven times here) keeping all parameters like gain, time for trajectory generation, minimum cable tensions unchanged. The end-effector was commanded to trace a circle of r = 0.15 meter radius and centered at the origin (center of the base plate) while attempting to maintain $\phi = 0$ for all motion in 10 seconds. Figure 18 shows the commanded trajectory (circle) with solid black line and actual trajectories generated by the CDDR shown with different colors.

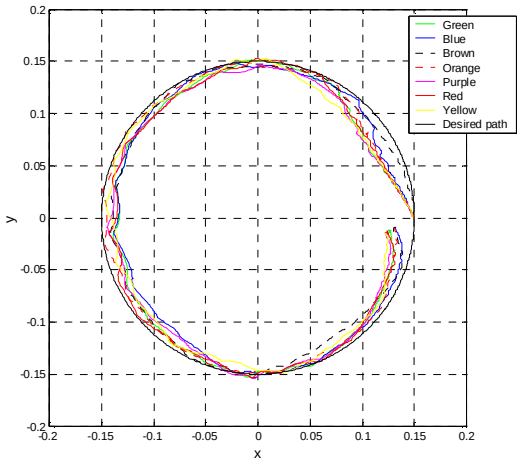

Figure 18: Repeatability of the CDDR

It can be seen that repeatability of the CDDR is good. The major source of error in repeatability could be the initial position and orientation of the end-effector as end-effector was placed manually at its initial position.

6 Conclusion

Hardware results were presented for the planar translational cable direct driven robot with three degree of freedom (x,y,ϕ commanded to 0) and one degree of actuation redundancy (4 cables but 3 Cartesian dof). Kinematics and statics modeling were implemented along with the method to maintain positive cable tensions successfully. Only translational CDDR is considered; attempt has been made to keep zero orientation by control. Results were presented for two linear trajectories and one circular trajectory. It was found that the whole theoretical statics workspace could not be used in hardware as it was difficult to move the end-effector in the region close to the edges of the statics workspace as it was approaching to singularity on the edges of the workspace where cable needs infinite force to move the end-effector, which can be major source of error in trajectory generation. It was also found that repeatability of the CDDR is quite good and a possible source of error could be the initial position and orientation of the end-effector as the end-effector was placed manually at its initial position. The future CDDRs should be designed taking into account the reduction in workspace due to singularity. The results revealed the need to implement the dynamics of the robot in the future for better performance. It was also found that there is a further scope of improvement in the performance of the robot, if the coordinated Cartesian controller could be used, by introducing vision system for online feedback of the Cartesian coordinates instead of independent length controller.

Acknowledgement

The authors gratefully acknowledge the assistance of Dr. Paolo Gallina of the University of Trieste, Italy, in computer simulations and design.

References

1. J.S. Albus, R. Bostelman, and N.G. Dagalakis, 1993, "*The NIST ROBOCRANE*", Journal of Robotic Systems, 10(5): 709-724.
2. P.D. Campbell, P.L. Swaim, and C.J. Thompson, 1995, "*Charlotte Robot Technology for Space and Terrestrial Applications*", 25th International Conference on Environmental Systems, San Diego, SAE Article 951520.
3. R. Lindemann and D. Tesar, 1989, "*Construction and Demonstration of a 9-String 6-DOF Force Reflecting Joystick for Telerobotics*", NASA International Conference on Space Telerobotics, (4): 55-63.
4. S. Walairacht, Y. Koike, and M. Sato, *"A new haptic display for both-hands-operation: SPIDAR-8"*, 1999 IEEE International Symposium on Intelligent Signal Processing and Communication Systems: 569-72.
5. S. Kawamura and K. Ito, 1993, "*New Type of Master Robot for Teleoperation Using a Radial Wire Drive System"*, Proceedings of the IEEE/RSJ International Conference on Intelligent Robots and Systems, Yokohama, Japan, July 26-30, 55-60.
6. R.L. Williams II, 1998, *"Cable-Suspended Haptic Interface"*, International Journal of Virtual Reality, 3(3): 13-21.
7. R.L. Williams II, Paolo Gallina, Jigar Vadia, 2002 "Planar Translational Cable-Direct-Driven-Robots", Journal of Robotic Systems (submitted)
8. R.G. Roberts, T. Graham, and T. Lippitt, 1998, "*On the Inverse Kinematics, Statics, and Fault Tolerance of Cable-Suspended Robots*", Journal of Robotic Systems, 15(10): 581-597.
9. R.L. Williams II and P. Gallina, "*Planar Cable-Direct-Driven Robots: Design for Wrench Exertion*", Journal of Intelligent and Robotic Systems, final manuscript, October 2001.
10. W. Choe, H. Kino, K. Katsuta, and S. Kawamura, 1996, *"A Design of Parallel Wire-Driven Robots for Ultrahigh Speed Motion Based on Stiffness Analysis"*, ASME Japan/USA Symposium on Flexible Automation, 1:159-166.
11. S. Kock and W. Schumacher, 2000, "*Control of Fast Parallel Robot with a redundant Chain and Gearboxes: Experimental Results"*, IEEE International Conference on Robotics and Automation: 1924-1929.
12. G. Barette and C.M. Gosselin, 2000, "*Kinematic Analysis and Design of Planar Parallel Mechanisms Actuated with Cables*", ASME Design Technical Conferences, Baltimore, MD.
13. Y. Shen, H. Osumi, and T. Arai, 1994, *"Manipulability Measures for Multi-wire Driven Parallel Mechanisms"*, IEEE International Conference on Industrial Technology, 550-554.
14. L.W. Tsai, 1999, Robot Analysis: The Mechanics of Serial and Parallel Manipulators, Wiley, New York.
15. C.M. Gosselin, 1996, "Parallel Computation Algorithms for the Kinematics and Dynamics of Planar and Spatial Parallel Manipulators", *Journal of Dynamic Systems, Measurement, and Control*, 118(1): 22-28.
16. F.L. Lewis, C.T. Abdallah, and D.M. Dawson, 1993, Control of Robot Manipulators, MacMillan, New York.
17. J.J. Craig, 1989, Introduction to Robotics: Mechanics and Control, Addison Wesley Publishing Co., Reading, MA.